

## Article

# Combined Application of Hydrogeological and Geoelectrical Study in Groundwater Exploration in Karst-Granite Areas, Jiangxi Province

Jacob Lubang<sup>1</sup>, Haifei Liu<sup>1,2,\*</sup> and Rujun Chen<sup>1,\*</sup> 

<sup>1</sup> Hunan Key Laboratory of Nonferrous Resources and Geological Hazards Exploration, Key Laboratory of Metallogenic Prediction of Nonferrous Metals, Ministry of Education, Innovation and Entrepreneurship Education Center for AIoT, Geology and Geophysics, School of Geosciences and Info-Physics, Central South University, Changsha 410083, China

<sup>2</sup> Team 416, Hunan Provincial Bureau of Geology and Mineral Exploration and Development, Zhuzhou 412003, China

\* Correspondence: liuhaifei@csu.edu.cn (H.L.); chrujun12358@gmail.com (R.C.)

**Abstract:** Drinking water shortage is a major concern in villages across southern Jiangxi, and this has impacted economic and social development. In order to address this challenge, groundwater prospecting was carried out in the villages under the support of Drinking Water Safety Project of China Geological Survey. In this study, we present two example sites in Ningdu County selected to demonstrate the combined hydrogeological survey, and the direct current electrical resistivity method was utilized for the present study for groundwater exploration in karst-granite distribution areas. First, a hydrogeological study was effectively used to delineate shallow severely weathered structural fissures as prospective target water-bearing beds. Then, a direct current electrical resistivity survey was used to confirm the distribution, thickness scale, and water-bearing features. The structural fractured zone whose distribution and trend were first established through hydrogeological surveys and whose development characteristics and water-richness were investigated by the direct current electrical resistivity method is the target layer for water exploration in the karst-granite rock areas. The water-bearing fracture zone shows a groove or strip-shape low resistivity anomaly and can be identified in its aquifer position according to its IP half decay time ( $T_h$ ), apparent polarizability ( $\eta_s$ ), and apparent resistivity ( $\rho_s$ ). The findings demonstrate that the above methods were successful in locating water potential areas, providing information for comparison and accurate borehole positioning. The results of the subsequent drilling and pumping tests supported the interpretation of the geophysical exploration data, and the water output from both boreholes met the objectives of this study. This groundwater search might serve as a guide for future exploration projects in similar areas.

**Keywords:** southern Jiangxi Province; hydrogeological survey; direct current prospecting; groundwater exploration; fault structure



**Citation:** Lubang, J.; Liu, H.; Chen, R. Combined Application of Hydrogeological and Geoelectrical Study in Groundwater Exploration in Karst-Granite Areas, Jiangxi Province. *Water* **2023**, *15*, 865. <https://doi.org/10.3390/w15050865>

Academic Editor: Ahmed Ismail

Received: 21 December 2022

Revised: 9 February 2023

Accepted: 16 February 2023

Published: 23 February 2023



**Copyright:** © 2023 by the authors. Licensee MDPI, Basel, Switzerland. This article is an open access article distributed under the terms and conditions of the Creative Commons Attribution (CC BY) license (<https://creativecommons.org/licenses/by/4.0/>).

## 1. Introduction

Water scarcity is posing a serious obstacle to both reclamation and cultivation of newly discovered land as well as irrigation of already reclaimed land, which could lead to desertification of the entire planet. Groundwater exploration is one strategy for resolving the challenges of limited water supplies around the world. As an old revolutionary base area, the economic development of southern Jiangxi is lower than the national average and is a designated poverty alleviation area by the Ministry of Natural Resources, where a lack of water resources is one of the main reasons for the economic backwardness [1]. The area has a large rural population base and is widely distributed. Some villages have serious seasonal water challenges all year round, and, in times of drought, people and animals face shortages due to shallow surface water. As a result, efforts to explore more

groundwater resources may help to find a solution to the problems of population expansion and surface water scarcity. Additionally, it is crucial to look for both quality and quantity of groundwater resources for sustainable development. As a result, aquifer quality, hydraulic properties, and thickness are the main factors that determine how groundwater aquifers develop and how management decisions affect agricultural management [2]. Therefore, choosing a scientific and reasonable method to survey and then quickly find a water source to meet the local economic and social development has become an important aspect of the district's poverty eradication and rural revitalization.

The methods used in groundwater exploration both domestically and abroad have certain similarities and universality, and they are used to explore groundwater sources either by geological or geophysical methods and then verified by drilling works [3,4]. The geological methods used include hydrogeological survey, geological survey mapping, remote sensing [5], etc., while the geophysical methods include conventional DC methods (joint profile method, ERT method, induced polarization (IP), natural electric field method, charging method, resistivity logging, etc.) and electromagnetic methods (transient electromagnetic method, magnetotelluric method, controlled source audio magnetotelluric method, etc.) [6,7]. From the perspective of a single electrical method, the electrical resistivity tomography (ERT) method is an effective tool to investigate hydrogeological characteristics of subsurface materials and has been used successfully in granite distribution areas [8–10], metamorphic rock distribution areas [11,12], and karst development areas [13–16]. Applications of these methods have increased due to advancement in data acquisition techniques, interpretation techniques, and computer technology [17–19]. Self-potential (SP) surveys, resistivity, and induced polarization (IP) are the commonly used geophysical methods to map the electrical properties of subsurface rock [20–24]. These methods have achieved good results in water search in Inner Mongolia [25] and Zhangjiakou in Hebei Province [26]. Use of the 2D resistivity imaging method has been suggested because of the lateral resistivity heterogeneity generally associated with weathered rocks [27]. The electrical logging method has provided reliable hydrogeological data for underground hydrogeological exploration and groundwater evaluation in Southern Syria and Hainan [28,29]; the comprehensive electrical method has also been widely used in groundwater exploration and has achieved better results in areas such as the “red layer area” in Sichuan [30], the Beishan area in Gansu [31], the karst area in Guizhou [32], the Qilian Mountains Formation water-scarce areas [33], Huaihua karst area in Hunan [34], etc. Further, refs. [35,36] used a combination of audio magnetotelluric sounding and high-density resistivity methods to detect the position, depth, scale, and occurrence characteristics of the deep water-bearing fault fracture zone in Figuil area (North Cameroon). The above literature provided effective technical support for design of hydrogeological drilling holes in this area. Based on the above, each method has its applicability and pertinence. To find groundwater efficiently and accurately, it is necessary to select the corresponding geophysical method according to the actual local conditions.

In this paper, based on previous works and research, two water-scarce locations were selected in karst-granite distribution areas of the Gannan region. The objective was to assess the hydrogeological materials and structures of the formation for groundwater search by combining hydrogeological survey and geoelectrical methods (DC method) and carry out target area selection of groundwater sources, thus meeting the water demands of water-scarce areas. According to the local geological and geomorphological conditions, we first carried out a hydrogeological investigation to determine the target aquifers and then carried out geophysical survey work by the DC method to circle the water-bearing favorable area and determine the location of boreholes. In later stages, drilling verification and pumping tests were carried out, and two borehole targets were drilled to produce domestic water that could meet the needs of local villagers. Through this exploration work, the structural development characteristics and groundwater aquifer structural characteristics of these villages were identified, the water richness was preliminarily judged, suggestions for drilling wells to find water were put forward, and the objectives and tasks of the project

were well accomplished. The above groundwater exploration methods and techniques provided references and guidance for implementing this water project.

## 2. Study Area Overview

### 2.1. Geomorphological and Geological Settings

The study area is located in the basin southwest of Ningdu County, Ganzhou City, Jiangxi Province in the upper reaches of Ganjiang River in the transition zone from the southeast coastal area to the central inland area and is an important passage from the inland to the southeast coast (Figure 1). It is located between coordinates latitude  $24^{\circ}29'–27^{\circ}09'$  N and longitude  $113^{\circ}54'–116^{\circ}38'$  E, with a total area of  $39,379.64 \text{ km}^2$ , accounting for 23.6% of the total area of Jiangxi Province. Climatologically, is located on the southern edge of the central subtropical zone and has a mild climate, abundant rainfall, and a long frost-free period. The maximum annual average temperature is  $18.8^{\circ}\text{C}$ , the annual average precipitation is 1605 mm, and the average frost-free period is 288 days. The topography is higher in the south and lower in the north. The mountains are undulating, and the rivers and streams are densely covered. The whole area is classified according to the topography it belongs to: a secondary structure on the second uplift belt of the Neocathaysian system. The strata in the area include Precambrian and Cambrian, Cretaceous, Jurassic, Quaternary, Carboniferous, mudpan, Permian, and magmatic, and there are many Precambrian–Cambrian and Cambrian magmatic rocks. The remaining strata are sporadically distributed [37]. The terrain is similar to the palm of a hand, high around and low in the middle, gradually sloping from the southeast to the northwest. The landform types are mainly denudation structure hills and erosion structure mountains, and the area of hills and low mountains accounts for about 80% of the region's total area.

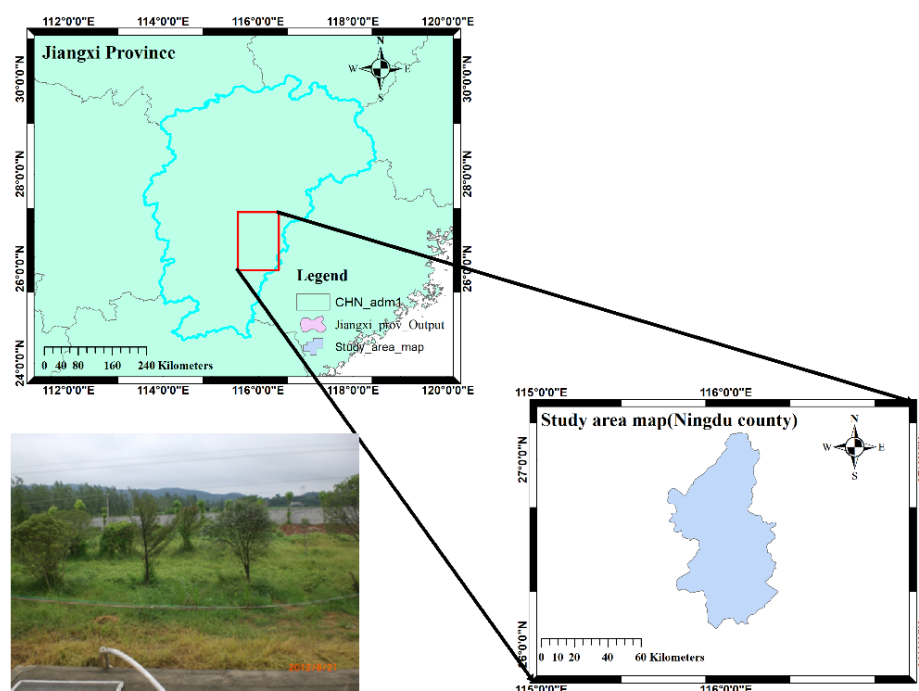


**Figure 1.** A brief map showing the location of the study area.

The regional geological structure belongs to the complex east–west tectonic belt of the Nanling Mountains. The NE trending faults are the most developed in the region and are distributed everywhere. It was mainly formed in the Caledonian period and further developed or sheared in later periods, especially the Yanshanian period. The sedimentary distribution of Cretaceous strata is mostly compressive and compressive–torsional, with an extensional length of about 10–54 km in general and large regional NE–NS trending faults strike with an angle of inclination  $45–80^{\circ}$  and width range 3–50 m. Structural traces are

compressive and torsional faults that cut and affect the distribution of Sinian and Cambrian strata and control the strike of Yanshanian granites and the extension of Cretaceous red bed basins [38].

The lithological characteristics, thickness, and distribution of each stratum in the survey area include a large area of magmatic rocks that can be seen outcropping with multiple phases, mainly Jurassic granite rock bases followed by dykes, specifically Early Jurassic fine-to-medium-grained porphyritic biotite granites, di-mica granites, and Middle Jurassic fine-medium-grained di-mica granites, biotite granites, and biotite granodiorites rock. In the periphery of the study area, the interbeds are composed of Lower Sinian system light grey, grey–white variegated fine-grained tuffaceous sandstone, tuffaceous silt, sedimentary tuff, and tuffaceous slate, as well as Lower Cretaceous Ganzhou Formation sandy conglomerate sandwiched with feldspar sandstone and shale with conglomerate, basalt, and tuff at the bottom [39]. The stratigraphy succession of the geological formations of the study area is presented (Figure 2).

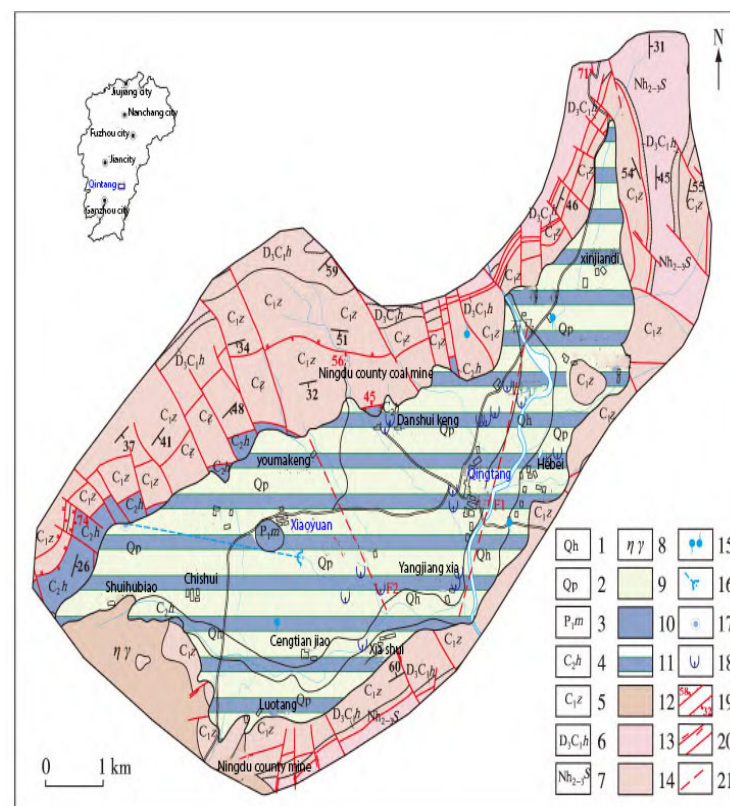


**Figure 2.** Hydrogeological map of the study area (modified after [40]). 1. Quaternary Holocene; 2. Quaternary Pleistocene; 3. Permian Mapping Formation; 4. Huanglong Formation of Carboniferous; 5. Carboniferous Zishan Formation; 6. Devonian–Carboniferous Huashan Formation; 7. Shanghai Formation of Nanhua System; 8. Yanshanian rock mass; 9. loose rock water-bearing rock group; 10. carbonate water-bearing rock group; 11. overburden carbonate water-bearing rock group; 12. magmatic water-bearing rock group; 13. metamorphic water-bearing rock group; 14. clastic water-bearing rock group; 15. ascending/descending spring; 16. a hidden river and an outlet; 17. a dark river skylight; 18. karst collapse; 19. measured normal fault, reverse fault, and occurrence; 20. measured translational fault, unknown nature fault; 21. presumed fault.

## 2.2. Regional Hydrogeological Background

Understanding hydrological properties is crucial for many applications, such as groundwater resource management and subsurface solute transport assessment. In the study area, groundwater types were classified according to the occurrence conditions, hydraulic properties, and hydraulic characteristics of groundwater; the groundwater is

divided into the following four types: loose rock pore water, clastic rock pore water, carbonate karst water, and bedrock pore water media. The pore water of loose rocks occurs in Quaternary Pleistocene and Holocene. The Pleistocene and Holocene systems are fluvial alluvial facies, distributed in discontinuous bands on both sides of the river. The Pleistocene consists of river terraces II, III, and IV, and the Holocene mainly consists of the river I terraces and side banks. The thickness of the aquifer is generally 0.55–5.58 m, and the average thickness of the aquifer is 3.15 m. The basin is located in the southwest of Ningdu County, Ganzhou City, Jiangxi Province. It is an NE-trending syncline basin with a length of about 10 km and a width of about 5 km. The Zishan Formation ( $C_1z$ ) is distributed symmetrically, and the core is composed of the Carboniferous Huanglong Formation ( $C_2h$ ) and the Permian Mapping Formation ( $P_1m$ ) (Figure 2). During the ground survey, it was found that the groundwater in the underlying karst basin in the basin broke through the overlying Quaternary system and overflowed the surface, forming karst rising springs. Therefore, this area is a covered karst-confined basin. The groundwater in this area flows from the mountains on both sides to the basin and develops asymmetrically; the mountains on the north side are high and rich in groundwater supply. Through the water conduction effect of the NW-trending extensional faults, the karst groundwater in this area is supplied by abundant bedrock fissure water. After flowing through the basin, it is finally discharged from the Shuikou polder. When the groundwater around the basin flows continuously into the basin, controlled by development of limestone karst water layers, most of the groundwater gathers into the basin along various channels, forming a confined aquifer with limestone at the top and the syncline axis at the bottom and concentrated discharge in the form of springs near the syncline axis (Figure 3). In areas where the Quaternary overburden is thin, the confined water breaks through the Quaternary alluvium along the fissures to form karst rising springs, while in the distribution area of the Quaternary are residual slope deposits of clay and clay gravel; because of their large thickness, slightly cemented, with strong water-repelling ability, it is generally not difficult to form karst rising springs. Karst springs are mainly distributed in the axis of limestone syncline basins, and the flow rates of springs in the recharge, runoff, and discharge areas are quite different. The flow rate of most springs is 1–10 L/s; the water inflow of most single wells is more than 1000 m<sup>3</sup>/d; the flow rate of underground rivers and large springs is 10–100 L/s; the runoff modulus is generally 1.98–7.41 L/s·km<sup>2</sup>, the average value is 4.42 L/s·km<sup>2</sup>, which is a medium amount of water.

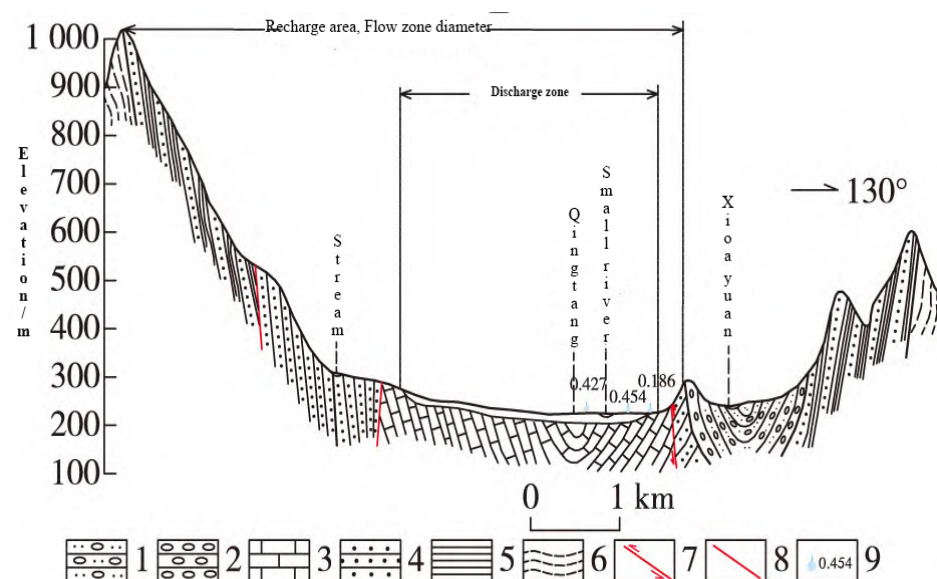


**Figure 3.** Hydrogeological cross-section map of recharge area, runoff, and discharge area in the study area (adopted after [40]). 1. Sandy conglomerate; 2. conglomerate; 3. limestone; 4. sandstone; 5. shale; 6. phyllite; 7. compressive fracture; 8. unknown fracture in nature; 9. rising spring and discharge.

### 3. Methods and Techniques for Groundwater Exploration

The targeted location is a basin located in the southwest of Ningdu County, Ganzhou City, Jiangxi Province, and local areas are Qingtang Middle School and Xiaoyuan Village, all under the jurisdiction of Ningdu County. The two survey areas are karst-granite areas, and, due to seasonal influence, there is no guaranteed production of safe drinking water. According to the actual situation of the site, the study is carried out according to the local conditions. The aspects of groundwater exploration work include: (1) to carry out hydrogeological surveys, mainly to clarify the direction of water search points, water-bearing formation, its extension, hydraulic parameters, groundwater quality assessment, and determine the geophysical detection line; (2) selecting geophysical prospecting methods and designing working parameters; (3) comprehensive geophysical data processing, interpretation, designing borehole drilling location, and carrying out groundwater assessment.

#### 3.1. Hydrogeological Survey

Combined with the geological background and topography of the study area and other local conditions plays an important role in groundwater characterization [41], hydrogeological investigations were carried out and the water-rich zones of the study area were determined through the investigations. The water-bearing rock group in the working area is mainly composed of Jurassic biotite granite, di-mica granite, dolomitic limestone, and limestone in the Middle Carboniferous system with clastic rocks in the Lower Carboniferous system, Sinian system on both sides and metamorphic rocks with good water-rich conditions. According to the local terrain, landform, geological structure, and lithological characteristics, the main groundwater types are judged. The main ideas are as follows: (1) in the granite gentle hill area, the terrain is relatively gentle and the thickness of the weathered layer is relatively thick, while granite outcrops are poor, fault structures and dyke structures are not easy to find, and it is difficult to find structural fissure water. The main direction of water search should be to search for weathered fissure water. (2) In granite karst areas, the topographical cutting is usually strong, the rocks are subject to weathering and denudation-erosion, the thickness of the weathered zone is small, and the topography is unconducive for enrichment of weathered fissure water. The conditions are good, and traces of fault structures and dyke structures are easier to find. Therefore, the search for fracture water in fault structures and dyke structures should be the main direction of water search. On-site hydrogeological surveys were carried out in the two survey areas, and the water search direction of each survey area was clarified; see Table 1 for details.

#### 3.2. Geophysical Survey

##### 3.2.1. Geophysical Characteristics

The lithology of the strata in the study area is a karst-granite distribution area, according to the regional geological data and preliminary physical exploration data (1:50,000 Jiangkou and Qingxi physical prospecting reports); combined with the field rock physical properties test of this geophysical exploration work, the geophysical characteristics were determined (Table 2). The electrical resistivity tomography (ERT) method has high efficiency, high data density, small point distance, and convenient construction, which can intuitively and accurately obtain an electrical anomaly from the underground target site and richer geological information about the characteristics of geoelectric section and improve interpretation accuracy, so the ERT method has obvious advantages in determining thickness of weathering layer in granite area. When granite mixed with sandstone or tuff contains a groundwater-filled fracture zone, the resistivity is relatively lower, forming a low-resistivity anomaly generally less than 100  $\Omega$  m. In the fracture zone, the joint profile curve is orthogonal anomalous features, or  $\rho_{sa}$ ,  $\rho_{sb}$  synchronous lower resistivity anomalous features; ERT method or apparent resistivity bathymetry contour forms low-resistance "V" type or uneven sparsity and other anomalous features. Therefore, there are obvious differences between the resistivity of the fractured zone filled with groundwater and the intact bedrock.

The above electrical differences provide a reliable geophysical prerequisite for electrical work. In the groundwater-filled tectonic fracture zone or relatively water-rich zone, the apparent resistivity curve ( $\rho_s$ ) in the joint profile method is characterized by inflection or platform-like anomalies, and the apparent polarization rate ( $\eta_s$ ), half-life time (TH), and attenuation degree (D) are relatively high-value anomalies [39]. Therefore, there are obvious differences between the resistivity of the groundwater-filled tectonic fracture zone and the intact bedrock. The joint profile method can observe the apparent resistivity from shallow to deep depth in the vertical direction and the corresponding change in apparent polarization rate, and the geological situation of the lower part of the measurement point along the vertical direction can be interpreted by analyzing the excitation bathymetry curve. Therefore, it is mostly used for water-richness exploration at different depths of fixed points. Based on the above geophysical characteristics, the combination of a hydrogeological survey and the direct current method is the ideal choice in this case.

**Table 1.** Hydrogeological conditions and groundwater prospecting directions.

Serial No.	Research Area	Hydrogeological Conditions	Water Search Direction
1	Qingtang Middle School, Ningdu County	The exploration area is located in an NE-trending corrosion syncline valley. There is an NE-trending fault structure (F1) in the area, and joints and fissures are relatively developed and the lithology exposed at the core is thick-layered massive dolomitic limestone and limestone in the middle Carboniferous system, with clastic rocks in the lower Carboniferous system and Sinian system on both sides, and metamorphic rock, with good water-rich conditions, karst development, and groundwater runoff from southwest to northeast.	Arranged 3 northwest survey lines to determine the northeast-trending fault structure and deep karst development zone in the syncline core.
2	Xiaoyuan Village, Ningdu County	A large area of granite is exposed nearby. According to the geological background conditions, a northeast-trending fault structure (F2) is developed in the exploration area; the terrain is flat. 700 m south of the target area is a fault valley. Joints and fissures are formed in the bedrock, and the thickness of the granite weathering crust is generally greater than 10 m. The groundwater is recharged by atmospheric precipitation and rivers laterally, and groundwater flows from northeast to southwest.	Arranged two survey lines to determine whether there is a northwest-trending secondary structure and find out the thickness of the weathered sand layer and water-richness of the granite. Mainly to find structural fissure water and granite weathering fissure water.

**Table 2.** Statistical summary table of physical properties of each geological body in the area.

Rock Layers	Apparent Resistivity Range ( $\Omega \cdot m$ )	Electromagnetic Wave Absorption Coefficient
Granite	600–6000 $\Omega \cdot m$	4.0–6.0
Carboniferous limestone	200–1000 $\Omega \cdot m$	1.0–3.0
Cretaceous glutenite interbedded with silty mudstone	100–400 $\Omega \cdot m$	1.0–3.0
Karst (filling)	400.0–800.0	1.0–3.0

### 3.2.2. Determining Geophysical Methods and Working Parameters

Field data acquisition and processing is one of the most important components of geophysical exploration. Based on the hydrogeological survey results and the geophysical characteristics of the target aquifer, geophysical lines were laid out in each of the two study areas using various methods (Table 3). The main target aquifer in Qingtang Middle School, Qingtang Town is granite weathering karst fissure water, so it is suitable to conduct electrical resistivity tomography (ERT) to investigate the thickness of weathering layer for the first step, and integrated use of joint profile and electrical resistivity tomography can further improve accuracy of interpretation. In Xiaoyuan Village, the target aquifer is

tectonic fracture water; therefore, the joint profile method was first used to investigate the development characteristics of the fault and then supplemented by electrical resistivity tomography method, which can greatly increase the success rate. To ascertain the thickness of the Quaternary and granite weathering layers in the gully in Qingtang Middle School, Ningdu County, three object detection lines (blue) are arranged in parallel along the northwest direction, and the numbers of the survey lines are numbered line 2, line 4, and line 6 in sequence (Figure 4). To identify the development characteristics of the fault at the bottom of the Xiaoyuan Village ditch, two nearly parallel northeast survey lines numbered lines 20 and 21 were laid out at the bottom of the ditch as the midpoint for tracing the direction of the structure, and the ERT and the joint profile method were used for exploration (Figure 5). In addition, a northwest survey line, numbered line 22, was arranged along the trench to supplement the exploration, and, to infer the extent of the secondary structure of the fault, ERT method was used this time. IP sounding was used to detect the water-richness of the weathered granite layer at the abnormal points.

Comprehensive geophysical survey of Qingtang Middle School, Qingtang Town, Ningdu County

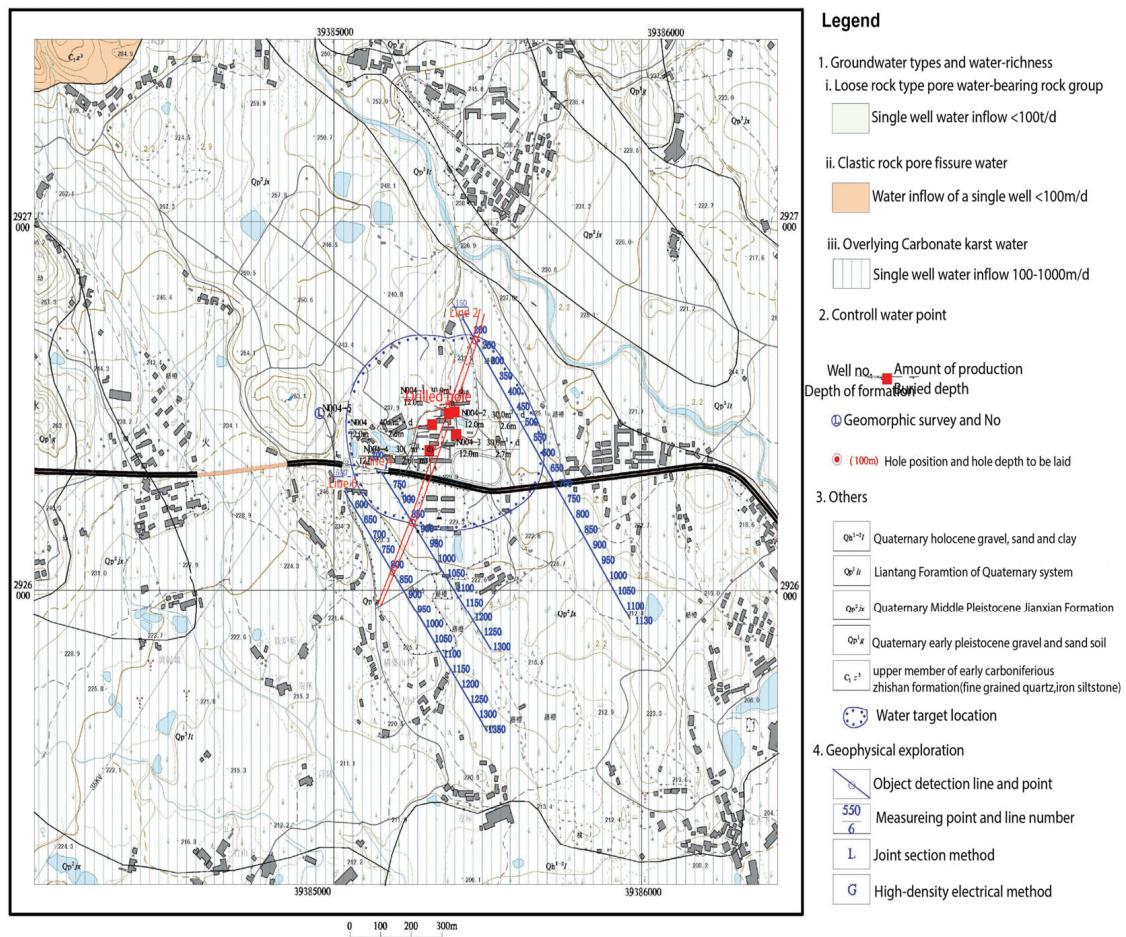


Figure 4. Hydrogeological map showing survey lines layout at Qingtang Middle School.

Comprehensive geophysical survey actual Material map of Xiaoyuan Vilalage, Dongdongba Town, Ningdu County

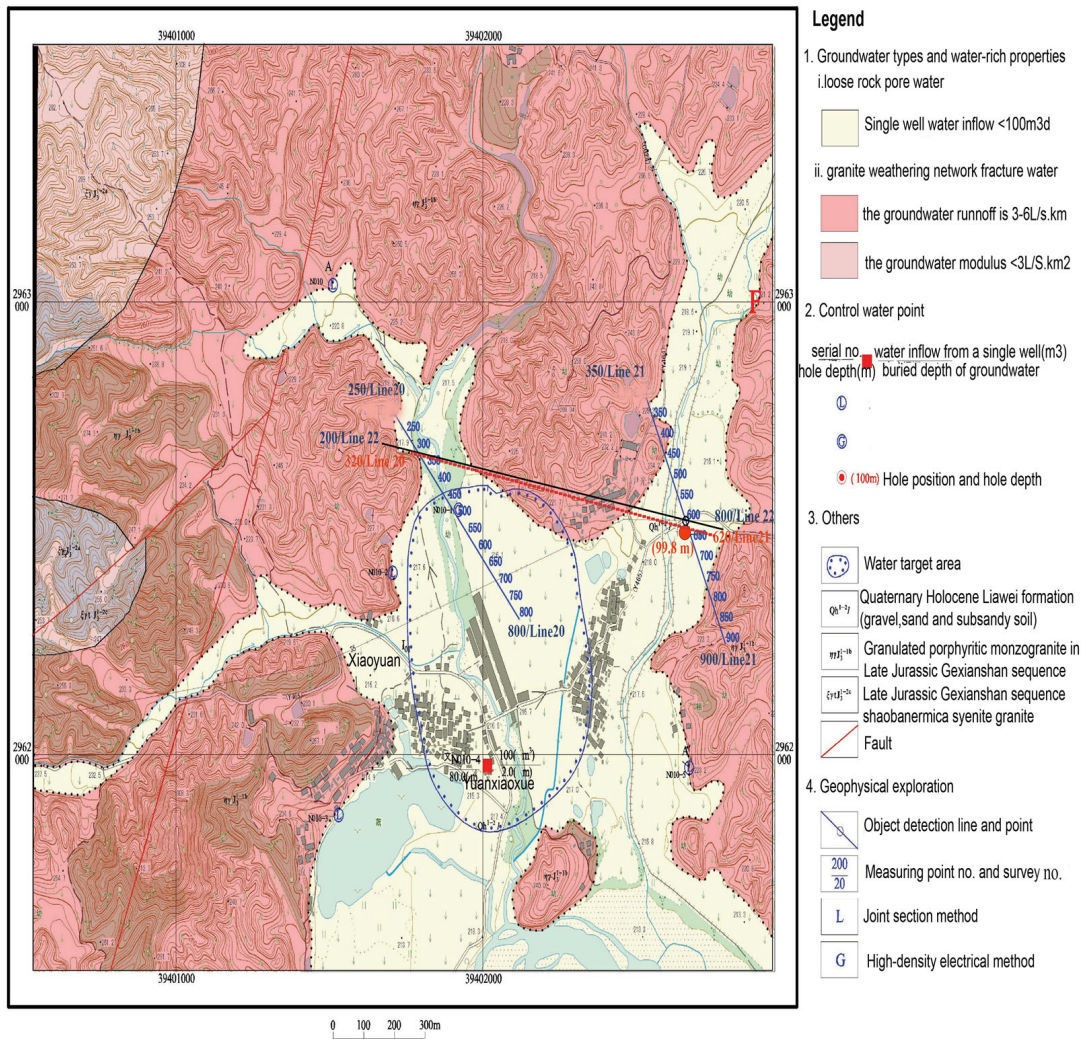
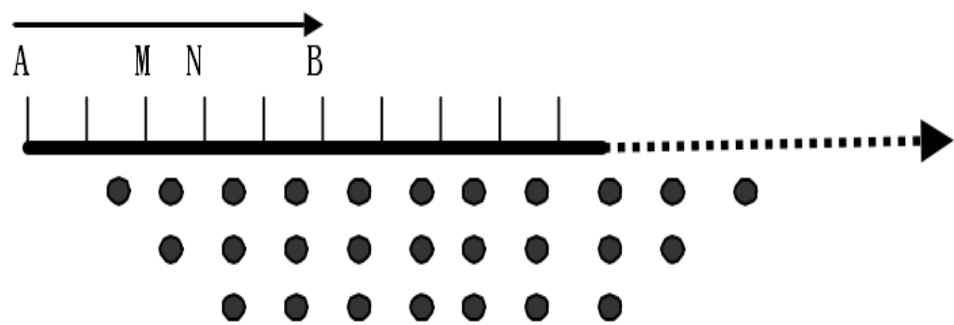


Figure 5. Hydrogeological map showing survey lines layout at Xiaoyuan Village.

Table 3. Survey lines layout in the study area.

Research Area	Line No.	Geophysical Method	Workload	Wiring Basis	Remarks
Qingtang Middle School, Ningdu County	2	Joint profile method	68	The relatively flat survey line can reduce the electrical resistivity tomography method interpretation error caused by the terrain height difference	The electrical resistivity method points distance of 10 m, and an interpretation depth of 0–120 m.
		Electrical resistivity method	120		
	4	Joint profile method	38		
		Electrical resistivity tomography method IP sounding	60 3		
Xiaoyuan Village, Dongshanba Town, Ningdu County	20	Joint profile method	38	The measurement line parallel to the inferred fault can increase the interpretation accuracy of the joint profile method; taking the bottom of the gully as the midpoint can make full use of the effective detection depth of electrical resistivity tomography method	The joint profile method points distance of 10 m, interpretation depth of 70 m, and 150 m.
		Electrical resistivity method	60		
	21	Joint profile method	38		
		Electrical resistivity tomography method IP sounding	60 2		

This geophysical exploration work is fast and effective from this angle. Joint profile and electrical resistivity tomography methods are the primary geophysical methods selected for this groundwater exploration work, supplemented by the IP sounding method. The ERT survey equipment used is the WGMD-4 high-performance electrical resistivity method developed by Chongqing Pentium Numerical Control Research Institute. The instrument has a unique and open measurement process that controls the power supply time and power outage time. The measurement process of each dataset can be flexibly selected. The joint profile method is designed with two pole distances with minimum pole distance 70 m and maximum pole distance 150 m and point spacing 20 m. To ensure the electrical resistivity method has a certain detection depth and anomalies do not shift in the lateral direction for improving the signal-to-noise ratio, the electrical resistivity tomography (ERT) data were collected with the Wenner device configuration with 60 electrodes and a single point data were collected with a maximum spacing of 10 m. During measurement, the Wenner device ( $\alpha$ ) was chosen to measure the electrode arrangement; see (Figure 6) for details. The measuring section is an inverted trapezoid; during measurement,  $AB = BM = MN$  is an electrode spacing, and  $ABMN$  moves to the right point by point to obtain the first section line. Then  $AB$ ,  $BM$ , and  $MN$  increase the electrode spacing by one point,  $ABMN$  moves to the right simultaneously, and another section line is obtained. In this way, scanning and measurement are continued to receive an inverted trapezoidal section.



**Figure 6.** Schematic diagram of the measurement principle of the Wenner device ( $\alpha$ ).

### 3.3. Data Processing and Data Interpretation Methods

To suppress the data interference and improve the detection effect, processing was performed by filtering out poor-quality data and the fresh data were used as input to the DC IP inversion system IPInv developed by Central South University to process the electrical data and then draw the relevant results according to the processed data [42]. The data processing flow is as follows: (a) when the terrain fluctuation of the exploration line is significant for the joint profile method data, the ratio method is used to correct the terrain. Then, Grapher software is used to draw the joint profile apparent resistivity curves. Otherwise, no processing is performed directly. (b) For the electrical resistivity method, first, convert the original data files collected by the instrument into a file format that can be used for analysis and processing, and then remove factors such as excessive grounding resistance, surface steepness, and local inhomogeneous bodies in the section. On this basis, two-dimensional inversion of resistivity is performed. Finally, Surfer software is used to draw a contour map of the measured and inversion data [43].

Combine hydrogeological data analysis and interpretation of the geophysical prospecting results. The basis and principles of interpretation are: (a) determine the resistivity distribution range of surrounding rocks and water-bearing targets. (b) In the vicinity of water-bearing fault structures, joints fissures, and stratigraphic boundaries, the joint profile curves are characterized by a low-resistivity orthogonal point, or the  $\rho_{sa}$ ,  $\rho_{sb}$  curves are synchronously low-resistivity “V”-shaped. At the same time, in electrical resistivity tomography 2D contour maps, there are morphological features, such as gradient bands, staggered breaks, isomorphic distortions, and steep ridges. (c) Deeply excavate the hydro-

geological data information and strengthen the comprehensive interpretation and analysis of the joint profile curves and resistivity contour graphs.

#### 4. Analysis of Geophysical Results and Discussion

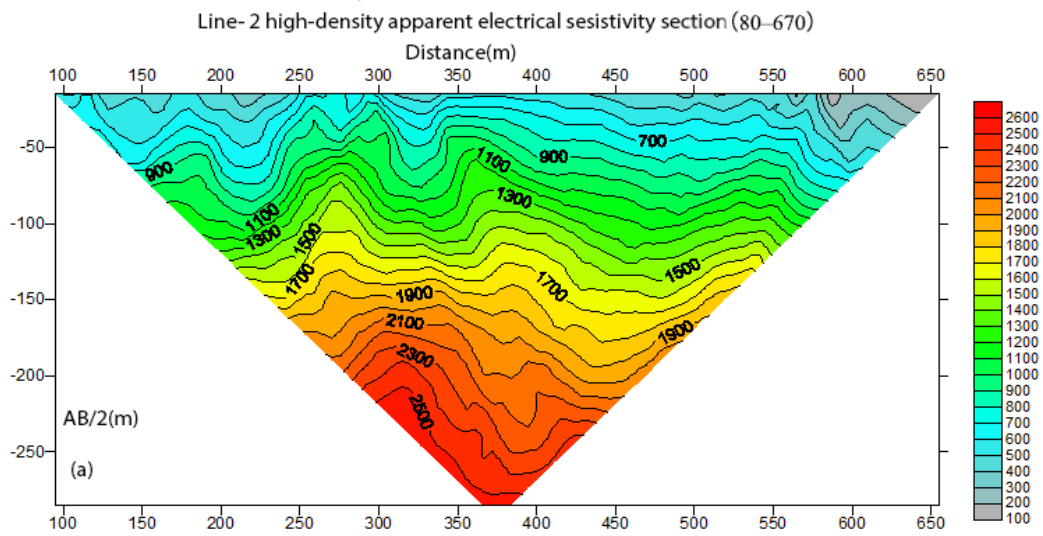
##### 4.1. Qingtang Middle School

The electrical resistivity tomography and the joint profile curve on line 2 (AO = 70 and 150) show a synchronous low-resistivity “V”-shaped anomaly near point 320 (Figure 7a,b); the electrical resistivity tomography cross-section on line 4 shows a low-resistivity anomaly near another point (Figure 7c), and the joint profile curve of line 6 shows an orthogonal point anomaly near points 825 and 1200 (Figure 7d). Combined with the plane map, it is assumed that the line connecting points 330 on line 2, point 920 on line 4, and point 825 on line 6 is the karst rift zone. The depth of the karst is presumed to be less than 120 m, and the thickness of overburden is 10–25 m [44]. Therefore, it is inferred that the above karst rift zone is the water-rich part of the survey area, and the Quaternary overburden in the covered karst area is 0–23.7 m. It is recommended that point 920 of line 4 is a relatively favorable water-rich section in Qingtang Middle School and a well was drilled here. To further evaluate the vertical geological information and water-rich conditions at the above-mentioned abnormal points, IP sounding surveys were carried out at points 900, 920, and 940 of line 4. From the IP sounding curves (Figure 7e), at  $AB/2 = 10$  m, 20 m, and 30 m, i.e., at depths of 20.0–30.0 m and 60.0–80.0 m, the apparent resistivity  $\rho_s$  presents a reflection or platform-like abnormal feature, while the apparent polarizability  $\eta_s$  shows a relative peak anomaly, which is inferred to be a water-bearing section with good water-rich properties [45]. Based on the results of geophysical prospecting and interpretation, it is recommended to drill water exploration wells at points 330 of line 2, 920 of line 4, and 825 of line 6 with a depth of 80.1 m.

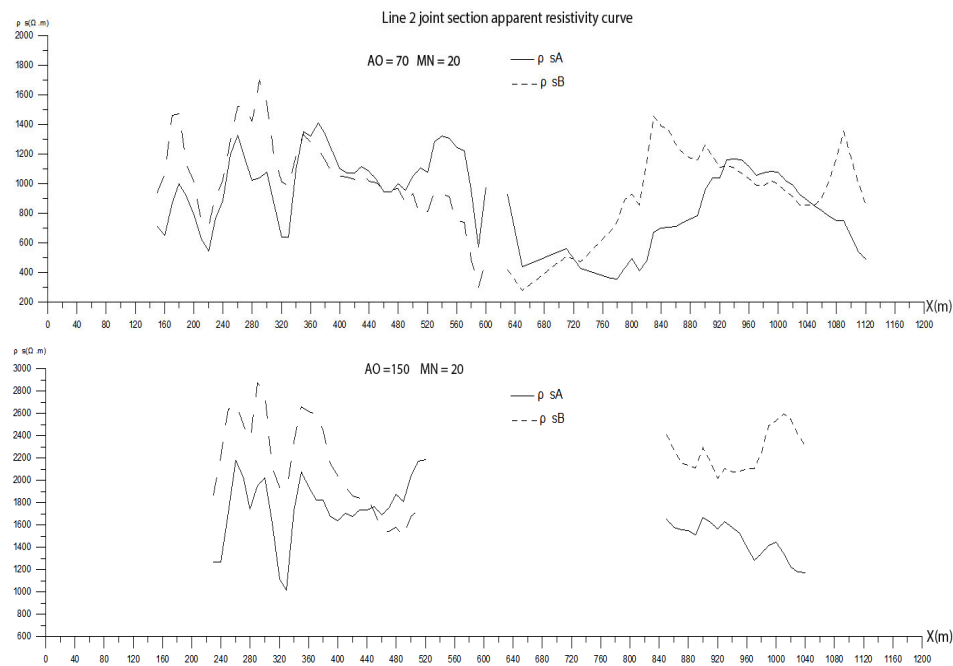
##### 4.2. Xiaoyuan Village

Affected by the dry sandy soil layer on the surface, the ground resistance is relatively large, and the geophysical interpretation effect is not ideal. According to the electrical resistivity tomography cross-sectional diagram and joint profile curve diagram on line 20, the local anomalies in the curve or sections point 330 were caused by some interference on the surface of this section because the surface was a riverbank. Therefore, no anomaly was found near line 20, section 330 is a relatively low-resistance zone in the shape of a strip. It is speculated that it may be a structural fissure zone or a fault fracture zone (Figures 8a and 9a). The structural plane dips to the northeast and is a favorable location for water [46]. At the same time, it is reflected on the resistivity inversion cross-section (Figures 8b and 9b), According to the cross-sectional diagram, the sand layer covering the surface is 6–8 m thick and contains a small amount of pore water. The joint profile curve (Figure 10a) near point 620 of line 21 shows an anomaly of orthogonal points, and the ERT shows a “V”-shaped resistance anomaly, and the deep anomaly is not obvious. It is inferred that the above position contains shallow weathered fissure water, and the thickness of the weathered sand layer is about 15 m. The southeast of point 330 on line 20 and point 620(ZK) on line 21 are recommended as drilling targets.

To infer its vertical geological information and water-richness on the faulted structural zone, combined with the electrical resistivity tomography apparent resistivity contour section map and the anomaly characteristics in the joint profile curve diagram, at point 330 on line 20 and point 620 line 21, the IP sounding method was carried out. Regarding the IP sounding curve (Figure 10b), the IP sounding curve at points 620–630 at  $AB/2 = 100$  m, 150 m, that is, at a depth of 6.1–18.2 m and 18.2–99.8 m, the apparent resistivity  $\rho_s$  presents a reflection or platform-like anomaly, and the apparent polarizability  $\eta_s$ , half-decay TH, and attenuation D present relative peak anomalies. It is recommended to conduct water exploration at this point at a borehole depth of 99.8 m.

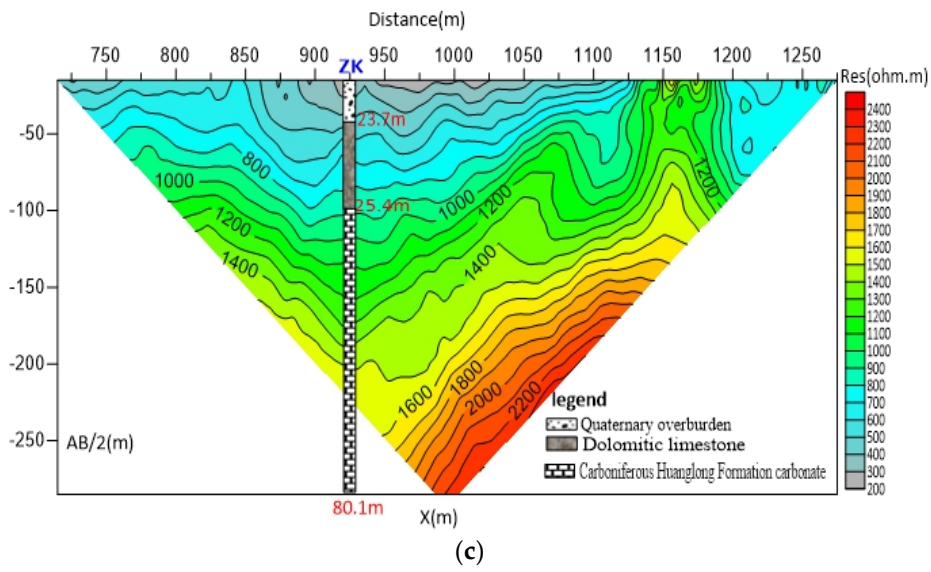


(a)



(b)

Figure 7. Cont.



Line 6 joint section apparent resistivity curve

AB/2 = 150 m MN = 20 m

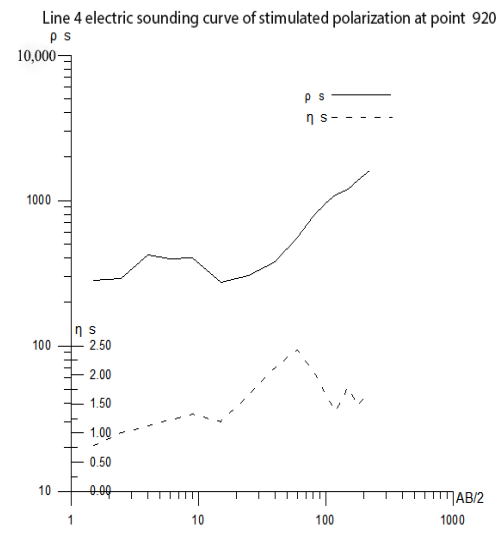
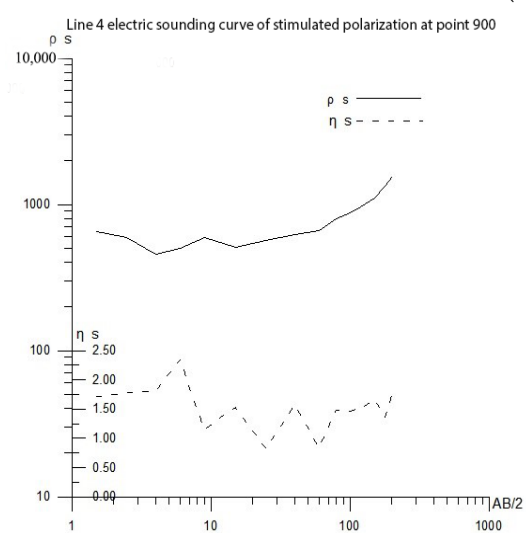
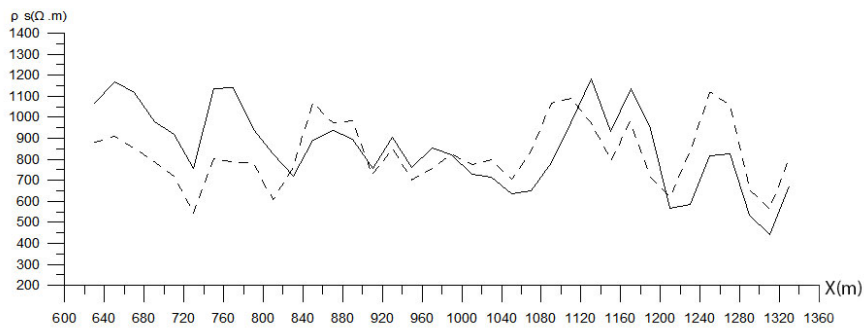
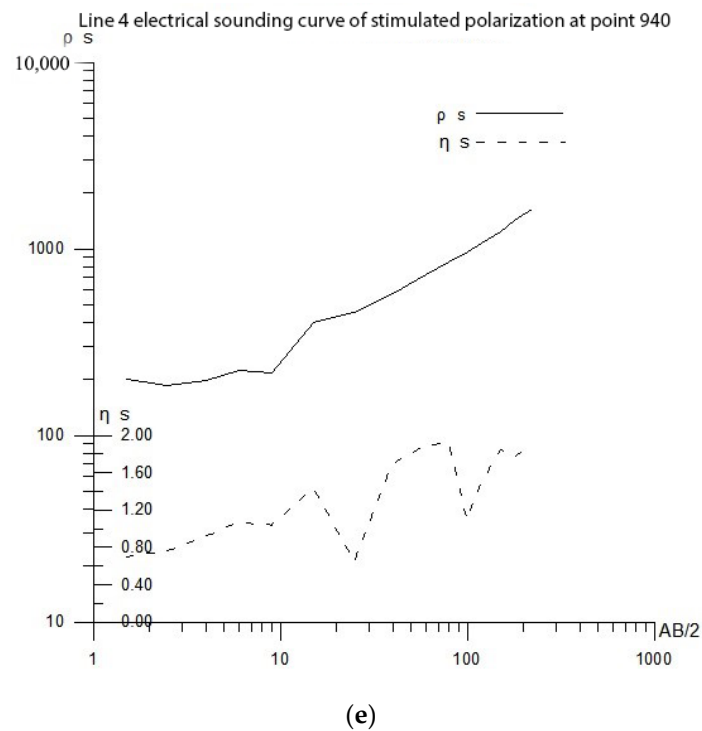
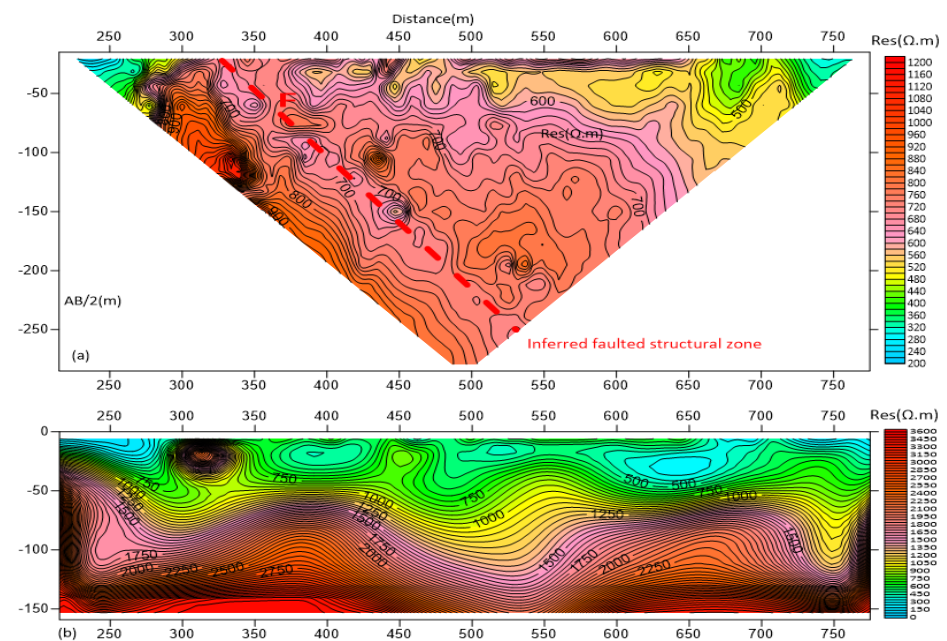


Figure 7. Cont.



**Figure 7.** Geophysical interpretation results at Qingtang Middle School, Ningdu County. (a) Electrical apparent resistivity cross-section line 2; (b) joint profile section curve 2; (c) electrical apparent resistivity section line 4; (d) joint profile section curve 6; (e) IP sounding curves stimulated at points 900, 920, and 940 on line 4.



**Figure 8.** High-density electrical method section of line 20 pseudo-section diagram of apparent resistivity: (a) pseudo-section diagram of apparent resistivity; (b) cross-section inversion section diagram of resistivity.

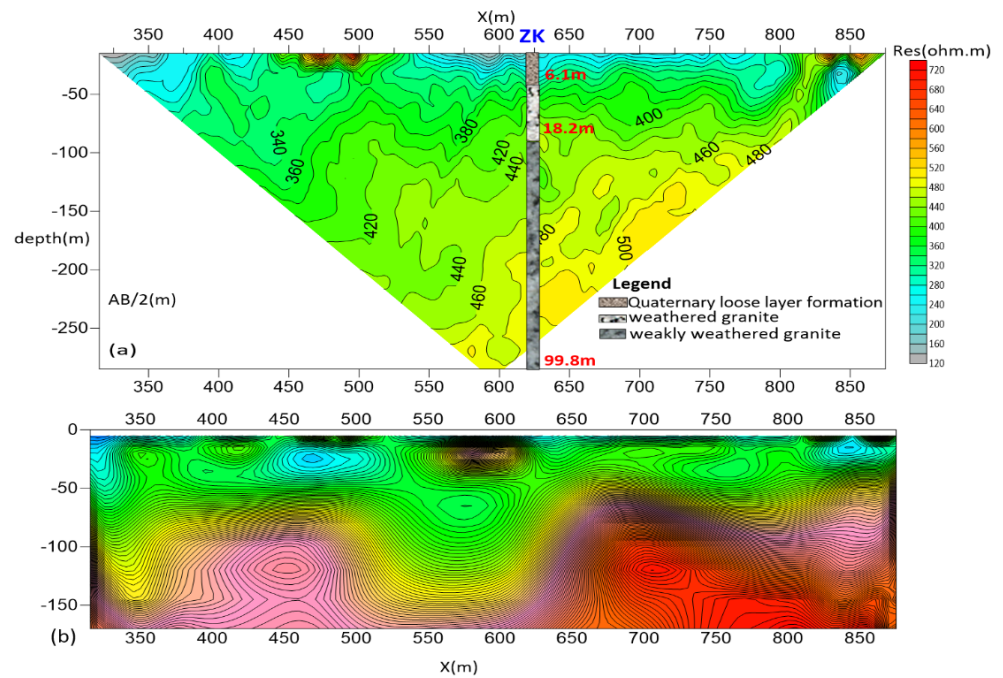


Figure 9. The electrical resistivity tomography (ERT method section of line 21 pseudo-section diagram of apparent resistivity: (a) pseudo-section diagram of apparent resistivity; (b) cross-section inversion.

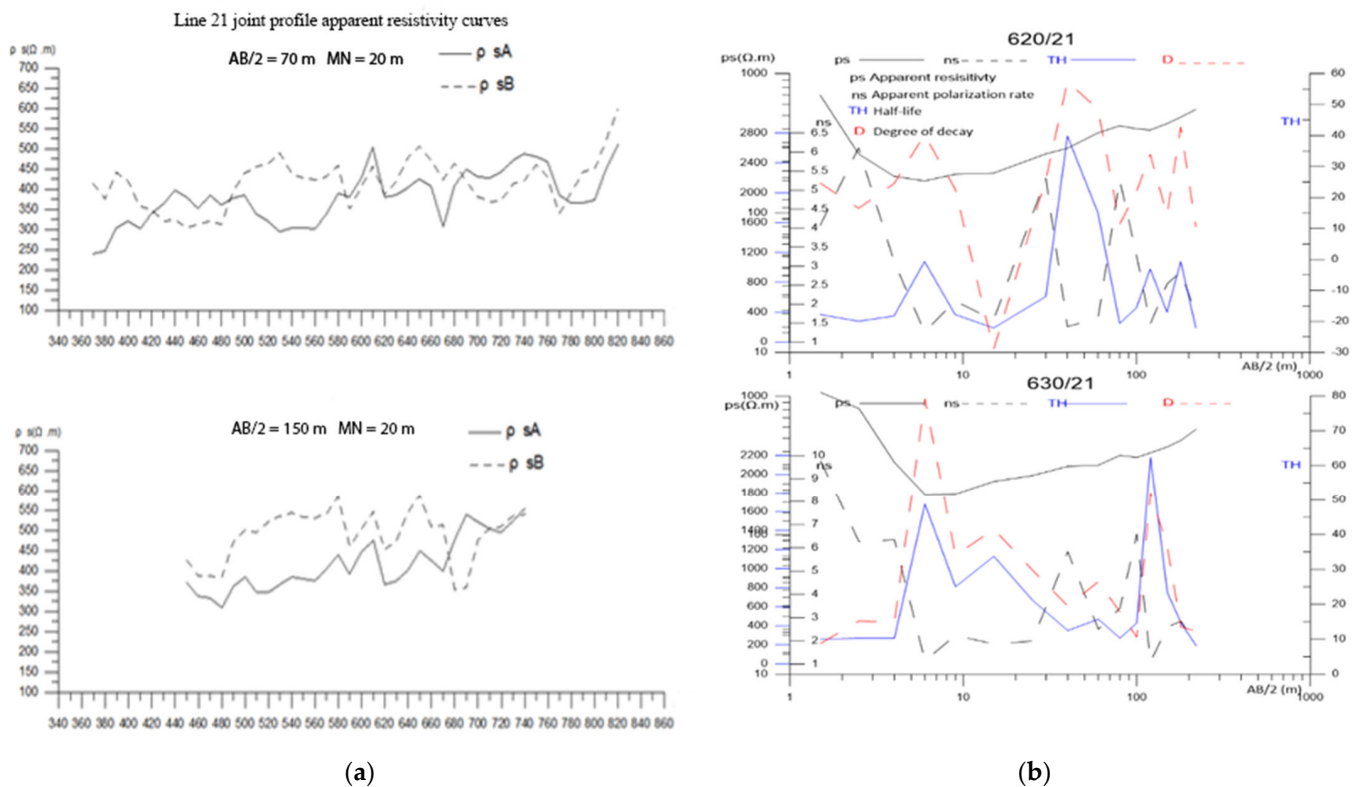


Figure 10. (a) Joint profile apparent resistivity curve line 21; (b) IP sounding result at points 620 and 630 of line 21.

## 5. Drilling Verification

### 5.1. Qingtang Middle School in Qingtang Town

The combined exploration and production well designed in Qingtang Middle School is located in the living area of Qingtang Middle School in West Qingtang Town, with geographical location coordinates  $115^{\circ}51'2.52''$  E,  $26^{\circ}26'36.78''$  N, and elevation of 233.12 m, which is convenient for transportation. The exploration–production combined well is located in the overburdened karst area, the Quaternary overburden is 0–23.7 m, and the 23.7–25.44 m section shows a 1.74 m mud-filled cave. The buried position of the cave is shallow, and the Quaternary overlay is thin. The geological conditions are poor. However, the ground observation within 300 m from the drill point during the construction and pumping process has not found any adverse environmental geological problems, such as surface natural wells and spring water points being plundered (fracture development zone). A well was drilled at the recommended point with a depth of 80.1 m, of which geological logs revealed that 25.44–80.1 m is carbonate karst water of the Carboniferous Huanglong Formation, with a thickness of 54.66 m. It is the main water intake layer of this “exploration–production combined well”. The drilling results are consistent with the geophysical interpretation. As verified by the pumping test, the measured maximum water inflow reached  $188.77 \text{ m}^3/\text{d}$ , and the water quantity and quality met the needs of Qingtang Middle School (see Table 4 for details).

### 5.2. Xiaoyuan Village, Dongshanba Town

Combined exploration and production wells with drilled depth of 99.8 m are designed in the area. It is located at longitude  $116^{\circ}01'16.92''$  E and latitude  $26^{\circ}46'11.10''$  N, with an elevation of 211.34 m, and the traffic is relatively convenient. The exposed strata are Quaternary and Yanshanian intrusive Jurassic granites, the Quaternary series is 0.5 m thick, and the main lithology is cultivated sandy soil, etc. The hole exposed 80.72 m of Jurassic granite, and the main lithology is granite (see Table 4 for details). The geophysical interpretation results show that drilling at point 330 on line 20 and point 620 on line 21 can achieve good results. Proven by the pumping test, the final water inflow is  $190.92 \text{ m}^3/\text{d}$ , and the metal silicate content is  $10.27 \text{ mg/L}$ , which meets the water supply requirements and achieves the work’s purpose. Regarding proposed mining volume, Xiaoyuan Village currently has a water-deficient population of about 3500 people. According to the acceptance criteria for safe drinking water in poverty alleviation in 2019, a drinking water volume of 40–60 L/person/day is basically up to the standard, and 60 L/person/day is fully up to the standard. A mining capacity of 180 tons per day can meet the acceptance requirements for safe drinking water. Calculating with reference to the long-term water quota of 100 L per person per day for rural residents, 300 tons per day of water can fully meet the drinking water needs of Xiaoyuan Village.

**Table 4.** Borehole description and pumping test results.

Serial No.	Survey Area	Description of Borehole Lithology and Water Content	Pumping Test and Drawing Volume Recommendations
1	Qingtang Middle School, Ningdu County	The depth of the hole is 80.1 m, of which 0–25.44 m is the pore water of the Quaternary loose rock formation, and the thickness is 25.44 m. The seamless steel pipe separates the water in this layer and is not taken. 25.44–80.1 m is Carboniferous Huanglong Formation carbonate karst water, with a thickness of 54.66 m, which is the main aquifer of this hole, with good water-richness, and is the main water intake layer of this “exploration–production combined well”.	From 05:54 on 12 October 2019 to 06:55 on 13 October 2019. The dynamic water level was 12.2 m, the triangular weir was 12.3 cm high, and the steady flow rate was $641.81 \text{ m}^3/\text{d}$ . The water volume is $188.77 \text{ m}^3/\text{d}$ .m., which fully meets the needs of the existing 1300 students and teachers.

Table 4. Cont.

Serial No.	Survey Area	Description of Borehole Lithology and Water Content	Pumping Test and Drawing Volume Recommendations
2	Xiaoyuan Village, Dongshanba Town, Ningdu County	<p>The drilled depth is 99.8 m. 0–6.1 m Quaternary loose layer formation, and the thickness is 0.5 m. The lithology of the aquifer is cultivated soil, etc., and the water-rich property is weak. Containing pore water-richness is water medium in nature; 6.1–18.2 m weathered granite, containing reticulated fissure water, strong water-richness with a thickness of 22.5 m; 18.2–99.8 m weakly weathered granite with joints and fissures with a thickness of 58.22 m, and the water-rich property is weak. The reticular fissure water in the granite weathering zone and the fissure water in the granite bedrock are the main aquifers in this hole and are the main water intake layers of this exploration–production combined well.</p>	<p>From 2–6 October 2019, the well was drawn down to a depth of 10.5 m and a steady flow rate of 968.4 t/d. A drinking water volume of 40–60 L/person per day is basically up to the standard, 60 L/person day or more is fully up to the standard, and the mining volume of 180 tons/day can meet the acceptance requirements for safe drinking water. Calculating with reference to the long-term water quota of 100 L per person per day for rural residents, 300 tons per day of water can fully meet the drinking water needs of Xiaoyuan Village. To sum up, the current number of people in Xiaoyuan Village who are short of water is 3500 people; it is recommended that the mining volume should not exceed 300 tons per day.</p>

5.3. Groundwater Assessment

Hydraulic Parameters and Pumping Test  
Qintang Middle School and Xiaoyuan Village

The supply, runoff, and discharge conditions of groundwater in the study area are mainly controlled by various factors such as meteorology, hydrology, topography, lithology, and structure. The general characteristics of groundwater recharge, runoff, and discharge conditions can be summarized as “near-ground recharge, short-path flow, and depression discharge”. The pore water of the Quaternary loose rock formation in this hole is mainly supplied by atmospheric precipitation, and the runoff direction is northeast to southwest, and it is discharged into the river at the low-lying place of Qingtang River. Limestone karst water supply sources of Carboniferous Huanglong Formation are relatively rich, including atmospheric precipitation, Quaternary loose rock formation water, rivers, carbonate karst water, etc. The main runoff direction is basically the same as that of surface water, from northeast to southwest. There are exposed cracks in rock formations and low-lying river discharges.

After construction is completed, observe the static water level according to the “Hydrogeological Handbook” and conduct the pumping test immediately after reaching the requirements. The static water level before pumping was 8.80 m, and the water level was drawn down and pumped three times (Table 5). According to the results of the steady flow pumping test, and according to the fact that the well type is a non-intact well with confined water, the following formula is used to calculate the permeability coefficient and influence radius of the exploration and production wells.

$$K = \frac{Q}{2\pi SM} \cdot \left( \ln \frac{R}{r} + \frac{M-L}{L} \ln \frac{1.12M}{\pi r} \right) \tag{1}$$

$$R = 10 S_w \sqrt{K} \tag{2}$$

From the formula: *K*—permeability coefficient (m/d), *R*—influence radius (m), *Q*—water inflow (m<sup>3</sup>/d), *S<sub>w</sub>*—water level drawdown value (m), *r*—pumping well radius (m), *L*—filter length (m), *M*—confined water aquifer thickness (m).

Specific method: assuming *R*0 = 100 m, substitute into Formula (1), use Formula (1) and Formula (2) to perform iterative calculation, and stop when the error of the two calculation results is less than 0.01 (see Tables 5 and 6 for specific calculation results).

**Table 5.** Results table of hydraulic parameters for three times depth reduction at Qingtang Middle School.

Drawdown $S_w$ (m)	Water Inflow $Q$ ( $m^3/d$ )	Test Section Thickness $H$ (m)	Pumping Well Radius $r$ (m)	Radius of Influence $R$ (m)	Permeability Coefficient $K$ (m/d)
$S_1 = 10.2$	737.09	54.66	0.074	199.41	3.822
$S_2 = 6.8$	709.03	54.66	0.074	157.27	5.349
$S_3 = 3.4$	641.81	54.66	0.074	102.83	9.147
Average value				153.17	6.106

**Table 6.** Results table of hydraulic parameters for three times depth reduction at Xiaoyuan Village.

Drawdown $S_w$ (m)	Water Inflow $Q$ ( $m^3/d$ )	Test Section Thickness $H$ (m)	Pumping Well Radius $r$ (m)	Radius of Influence $R$ (m)	Permeability Coefficient $K$ (m/d)
$S_1 = 10.5$	968.40	97.80	0.074	365.80	3.102
$S_2 = 7.0$	810.00	97.80	0.074	265.45	3.676
$S_3 = 3.5$	668.22	97.80	0.074	163.87	5.604
Average value				265.04	4.127

A total of three water level drawdowns were conducted: the first water level drawdown was completed from 06:20–18:21 on 10 October 2019. The  $S_1$  was 10.2 m, the dynamic water level was 19.0 m, the triangular weir was 13.0 cm high, and the steady flow rate was  $737.09 m^3/d$ . The water volume was  $72.26 m^3/d \cdot m$ . The second water level drawdown was completed from 02:52–20:53 on 11 October 2019. The  $S_2$  was 6.80 m, the dynamic water level was 15.6 m, the triangular weir was 12.8 cm high, and the steady flow rate was  $709.03 m^3/d$ . The water volume was  $104.27 m^3/d \cdot m$ . The third water level drawdown was completed from 05:54 on 12 October 2019 to 06:55 on 13 October 2019. The  $S_3$  was 3.4 m, the dynamic water level was 12.2 m, the triangular weir was 12.3 cm high, and the steady flow rate was  $641.81 m^3/d$ . The water volume was  $188.77 m^3/d \cdot m$ . After the pumping test, the recovery water level was observed immediately, and the recovery to stable water level time was 66 min, 46 min, and 46 min, respectively, and the recovery stability time was the same. Since it is dry season pumping, the water provided is guaranteed at a high degree in the state of exploitation.

At Xiaoyuan Village, the pore water of the Quaternary loose rock formation in this hole is mainly supplied by atmospheric precipitation, and the runoff direction is from west to east, and it is discharged into the river at the low-lying part of Huangpi River. The source of fissure water in the Jurassic granite bedrock is mainly atmospheric precipitation, followed by Quaternary loose rock formation water, etc. The main runoff direction is basically the same as that of surface water, which is southwest and north to east, where cracks are exposed in rock formations and low-lying rivers flows everywhere. After construction is completed, the static water level according to the “Hydrogeological Handbook” should be determined, and conduct the pumping test immediately after reaching the requirements. Before pumping, the static water level was 1.80 m, and a total of three times the water level was drawn down and pumped results are shown in (Table 6).

The first water level drawdown was completed from 06:00 on 3 October 2019 to 15:31 on 3 October 2019. The  $S_1$  was 10.5 m, the dynamic water level was 12.3 m, the height of the triangular weir was 14.5 cm, and the steady flow rate was  $968.4 m^3/d$ . The water volume was  $92.23 m^3/d \cdot m$ . The second water level drawdown was completed from 00:32 on 4 October 2019 to 17:33 on 4 October 2019. The  $S_2$  was 7.0 m, the dynamic water level was 8.8 m, the height of the triangular weir was 13.5 cm, and the steady flow rate was  $810.0 m^3/d$ . The water volume was  $115.71 m^3/d \cdot m$ . The third water level drawdown

was completed from 01:34 5 October 2019 to 01:55 6 October 2019. The S3 was 3.5 m, the dynamic water level was 12.2 m, the triangular weir was 12.5 cm high, and the steady flow rate was 668.22 m<sup>3</sup>/d. The water volume was 190.92 m<sup>3</sup>/d.m. immediately after the pumping test, the recovery water level observation was carried out, and the recovery time to a stable water level was 7 min. Since the water was pumped in the dry season, the amount of water provided is guaranteed to be relatively high under mining conditions.

## 6. Conclusions

Taking Qingtang Middle School, Qintang Town, and Xiaoyuan Village, Dongshanba Town, in Ningdu County, Ganzhou City, Jiangxi Province as examples, this paper discusses combined application of a hydrogeological survey with a comprehensive geophysical exploration method in groundwater search. The study has demonstrated that determination of a water-bearing target layer in a field hydrogeological survey is the basis of groundwater exploration. Adopting a geophysical exploration method suitable for a water bearing target layer can accurately and efficiently identify aquifer distribution, burial depth, structure, and water-bearing characteristics in an exploration area so as to provide data support for borehole location comparison and accurate positioning. It has good application prospects in water exploration and can provide a reference for future work in groundwater exploration.

**Author Contributions:** Formal analysis, H.L.; Resources, R.C.; Data curation, H.L.; Writing—original draft, J.L.; Writing—review and editing, R.C.; Visualization, H.L.; Supervision, R.C.; Funding acquisition, R.C. All authors have read and agreed to the published version of the manuscript.

**Funding:** This research was funded by the Basic Science Centre Project of the National Natural Science Foundation of China, Grant Number 72088101.

**Data Availability Statement:** Data supporting the reported results can be obtained from the authors upon reasonable request.

**Conflicts of Interest:** The authors declare no conflict of interest.

## References

- Huang, C.; Zhou, Y.; Zhang, S.; Wang, J.; Liu, F.; Gong, C.; Yi, C.; Li, L.; Zhou, H.; Wei, L. Groundwater resources in the Yangtze River Basin and its current development and utilization. *Geol. China* **2021**, *48*, 979–1000.
- El Osta, M.; El Sheikh, A.E.; Barseem, M. Comparative hydrological and geoelectrical study on the quaternary aquifer in the deltas of Wadi Badaa and Ghweiba, El Ain El Sukhna Area, Northwest Suez Gulf, Egypt. *Int. J. Geophys.* **2010**, *2010*, 585243.
- Zhang, S.; Jiang, P.; Lu, L.; Wang, S.; Wang, H. Evaluation of Compressive Geophysical Prospecting Method for the Identification of the Abandoned Goaf at the Tengzhou Section of China's Mu Shi Expressway. *Sustainability* **2022**, *14*, 13785. [[CrossRef](#)]
- Zhou, Y.; Jianwei, P.; Hao, L.; Zhongmei, W.; Jiang, Z.; Haixin, L.; Jiayu, L. Multi-turn small-loop transient electromagnetic data processing using constraints from borehole and electrical resistivity tomography data. *Arab. J. Geosci.* **2022**, *15*, 1675. [[CrossRef](#)]
- Sener, E.; Davraz, A.; Ozelik, M. An integration of GIS and remote sensing in groundwater investigations: A case study in Burdur, Turkey. *Hydrogeol. J.* **2005**, *13*, 826–834. [[CrossRef](#)]
- Lee, S.C.H.; Noh, K.A.M.; Zakariah, M.N.A. High-resolution electrical resistivity tomography and seismic refraction for groundwater exploration in fracture hard rocks: A case study in Kanthan, Perak, Malaysia. *J. Asian Earth Sci.* **2021**, *218*, 104880. [[CrossRef](#)]
- Kouadio, K.L.; Xu, Y.; Liu, C.-m.; Boukhalifa, Z. Two-dimensional inversion of CSAMT data and three-dimensional geological mapping for groundwater exploration in Tongkeng Area, Hunan Province, China. *J. Appl. Geophys.* **2020**, *183*, 104204. [[CrossRef](#)]
- Feng-Shan, M.; Qing-Yun, D.; Ke-Peng, L.; Chang-Min, F.; Shan-Fei, W.; Wei, L. Application of High-Density Resistivity Method in Detecting Water-Bearing Structures at a Seabed Gold Mine. *Chin. J. Geophys.* **2016**, *59*, 717–724. [[CrossRef](#)]
- Fang, H.; Tong, B.; Du, X. Integrated system of geophysical methods for shallow loose covering stratum exploration in the granite region in the northwest of Zhejiang Province, China. In Proceedings of the IOP Conference Series: Earth and Environmental Science, Beijing, China, 23–26 October 2020; p. 042018.
- Huang, Z.; Ran, T.; Dong, J.; Yuan, G.; Zhao, G. Study on Granite Permeability Zoning Based on Electrical Resistivity: Take Wuyue Pumped Storage Power Station as an Example. *Geofluids* **2022**, *2022*, 8288408. [[CrossRef](#)]
- Lin, Z.; Shi, Y.; Chong, J.; Ren, F.; Yan, Q.; She, T.; Shi, X.; Li, C. Using High-density Electrical Method to Detect the Yuehe Fault in the Site of Seismic Microzonation of Ankang City. In Proceedings of the IOP Conference Series: Earth and Environmental Science, Qingdao, China, 23–25 November 2018; p. 052058.
- Hervé, G.D.; Darolle, F.K.A.; Fidèle, K.; David, Y. Groundwater prospecting using remote sensing and geoelectrical methods in the North Cameroon (Central Africa) metamorphic formations. *Egypt. J. Remote Sens. Space Sci.* **2021**, *24*, 933–943.

13. Jianjun, G.; Zhang, Y.; Xiao, L. An application of the high-density electrical resistivity method for detecting slide zones in deep-seated landslides in limestone areas. *J. Appl. Geophys.* **2020**, *177*, 104013. [[CrossRef](#)]
14. Zhang, H.Q.; Cao, Z.B.; Li, W. Application of High Density Electrical Method in Karst Area. In Proceedings of the International Conference on Civil Engineering, Singapore, 21–23 January 2023; pp. 229–233.
15. Jingjing, C.; Changhong, Y.; Ning, W.; Yong, S.; Jun, Z.; Zhigang, T. Application of high-density resistivity method to karst investigation of metro engineering. *J. Eng. Geol.* **2011**, *19*, 935–940.
16. Yu, X.; Pei, F.; Han, J.; Gao, W.; Wang, X. Ordovician limestone karst development law in Feicheng coal field. *Environ. Earth Sci.* **2018**, *77*, 781. [[CrossRef](#)]
17. Binley, A.; Hubbard, S.S.; Huisman, J.A.; Revil, A.; Robinson, D.A.; Singha, K.; Slater, L.D. The emergence of hydrogeophysics for improved understanding of subsurface processes over multiple scales. *Water Resour. Res.* **2015**, *51*, 3837–3866. [[CrossRef](#)]
18. Loke, M.; Chambers, J.; Rucker, D.; Kuras, O.; Wilkinson, P. Recent developments in the direct-current geoelectrical imaging method. *J. Appl. Geophys.* **2013**, *95*, 135–156. [[CrossRef](#)]
19. Loke, M.H.; Barker, R.D. Rapid least-squares inversion of apparent resistivity pseudosections by a quasi-Newton method1. *Geophys. Prospect.* **1996**, *44*, 131–152. [[CrossRef](#)]
20. Revil, A.; Murugesu, M.; Prasad, M.; Le Breton, M. Alteration of volcanic rocks: A new non-intrusive indicator based on induced polarization measurements. *J. Volcanol. Geotherm. Res.* **2017**, *341*, 351–362. [[CrossRef](#)]
21. Jardani, A.; Revil, A.; Santos, F.; Fauchard, C.; Dupont, J.-P. Detection of preferential infiltration pathways in sinkholes using joint inversion of self-potential and EM-34 conductivity data. *Geophys. Prospect.* **2007**, *55*, 749–760. [[CrossRef](#)]
22. Jardani, A.; Revil, A.; Barrash, W.; Crespy, A.; Rizzo, E.; Straface, S.; Cardiff, M.; Malama, B.; Miller, C.; Johnson, T. Reconstruction of the water table from self-potential data: A Bayesian approach. *Groundwater* **2009**, *47*, 213–227. [[CrossRef](#)]
23. Schulz, R. Interpretation and depth of investigation of gradient measurements in direct current geoelectrics. *Geophys. Prospect.* **1985**, *33*, 1240–1253. [[CrossRef](#)]
24. Johnson, T.C.; Versteeg, R.J.; Ward, A.; Day-Lewis, F.D.; Revil, A. Improved hydrogeophysical characterization and monitoring through parallel modeling and inversion of time-domain resistivity and induced-polarization data. *Geophysics* **2010**, *75*, WA27–WA41. [[CrossRef](#)]
25. Enkhbold, A.; Khukhuudei, U.; Kusky, T.; Tsermaa, B.; Doljin, D. Depression morphology of Bayan Lake, Zavkhan province, Western Mongolia: Implications for the origin of lake depression in Mongolia. *Phys. Geogr.* **2022**, *43*, 727–752. [[CrossRef](#)]
26. Liu, Z.-y.; Tan, D.; Chen, Z.-b.; Wei, Y.-f.; Chai, Q.; Chen, X.-h. Study on multiple induced polarization parameters in groundwater exploration in Bashang poverty alleviation area of Heibei Province, China. *J. Groundw. Sci. Eng.* **2020**, *8*, 274–280.
27. Revil, A.; Hermitte, D.; Spangenberg, E.; Cochémé, J. Electrical properties of zeolitized volcanoclastic materials. *J. Geophys. Res. Solid Earth* **2002**, *107*, ECV 3-1–ECV 3-17. [[CrossRef](#)]
28. Asfahani, J. Basalt characterization by means of nuclear and electrical well logging techniques. Case study from Southern Syria. *Appl. Radiat. Isot.* **2011**, *69*, 641–647. [[CrossRef](#)]
29. Xu, H.; Yang, X.; Wang, D.; Hu, Y.; Cheng, Z.; Shi, Y.; Zheng, P.; Shi, L. Multivariate and spatio-temporal groundwater pollution risk assessment: A new long-time serial groundwater environmental impact assessment system. *Environ. Pollut.* **2022**, *317*, 120621. [[CrossRef](#)]
30. Wang, X.; Wang, X.; Wang, K.; Luo, W.; Xiao, J.; Hu, J.; Hu, D. Research on Internal Structure and Mechanism of Landslide Based on Hydrogeophysical Investigation (Quan'an Landslide, Southwest China). *Geofluids* **2022**, *2022*, 7843011. [[CrossRef](#)]
31. Lu, D.; Huang, D.; Xu, C. Estimation of hydraulic conductivity by using pumping test data and electrical resistivity data in faults zone. *Ecol. Indic.* **2021**, *129*, 107861. [[CrossRef](#)]
32. Zhang, M.; Yang, W.; Yang, M.; Yan, J. Guizhou Karst Carbon Sink and Sustainability—An Overview. *Sustainability* **2022**, *14*, 11518. [[CrossRef](#)]
33. Xiong, R.; Zheng, Y.; Han, F.; Tian, Y. Improving the scientific understanding of the paradox of irrigation efficiency: An integrated modeling approach to assessing basin-scale irrigation efficiency. *Water Resour. Res.* **2021**, *57*, e2020WR029397. [[CrossRef](#)]
34. Li, C.; Ding, J.; Liao, Y.; Lu, S. *Groundwater Chemical Kinetics and Fractal Characteristics of Karst Tunnel*; Springer: Berlin/Heidelberg, Germany, 2020.
35. Gouet, D.H.; Kana, J.D.; Guimbous, J.J.K.; Ewembe, F.Y.; Mbabi, A.; Ngos III, S. Remote sensing and DC electrical investigations in the Figuil area (North-Cameroon): Structural and geological implications. *NRIAG J. Astron. Geophys.* **2022**, *11*, 147–165. [[CrossRef](#)]
36. Cao, G.; Liu, H. *Three-Dimensional Exploration Technology of Tunnel Geology*; Springer: Berlin/Heidelberg, Germany, 2022.
37. Hu, R.-Z.; Zhou, M.-F. Multiple Mesozoic mineralization events in South China—An introduction to the thematic issue. *Miner. Depos.* **2012**, *47*, 579–588. [[CrossRef](#)]
38. Li, Z.-X.; Li, X.-H. Formation of the 1300-km-wide intracontinental orogen and postorogenic magmatic province in Mesozoic South China: A flat-slab subduction model. *Geology* **2007**, *35*, 179–182. [[CrossRef](#)]
39. Bo-Luo, O. Application of Hydrogeological Survey Combined with Direct Current Prospecting in Groundwater Search in Southern Jiangxi Province. *China Geol.* **2022**, *38*, 240–249, (In Chinese with English Abstract).
40. Liu, Q.; Huang, X.; He, W. Characteristics and exploitation divisions of karst water in Qingtang Basin, Southern Jiangxi. *East China Geol.* **2022**, *43*, 364–373.
41. Sonkamble, S.; Chandra, S.; Pujari, P.R. Application of airborne and ground geophysics to unravel the hydrogeological complexity of the Deccan basalts in central India. *Hydrogeol. J.* **2022**, *30*, 2097–2116. [[CrossRef](#)]

42. Tripp, A.C.; Killpack, T.J. *IPINV: A Two-Dimensional Dipole-Dipole Resistivity Modeling and Inversion Program; User's Guide and Documentation for Rev. 1*; Earth Science Lab., Utah Univ.: Salt Lake City, UT, USA, 1981.
43. Yang, G.L.; Liu, J.T.; Wang, Z. Application effect of data processing methods of direct current electrical sounding in groundwater exploration. *Resour. Environ. Eng.* **2008**, 610–613. (In Chinese with English Abstract)
44. Hasan, M.; Shang, Y.; Jin, W.; Akhter, G. Estimation of hydraulic parameters in a hard rock aquifer using integrated surface geoelectrical method and pumping test data in southeast Guangdong, China. *Geosci. J.* **2021**, 25, 223–242. [[CrossRef](#)]
45. Xu, Y.; Wang, H.-J.; Yin, J.-G.; Zhang, H.-L.; Li, G. The application of half decay time parameter of IP to exploration of underground water in the hilly area of Dongping. *Geophys. Geochem. Explor.* **2014**, 684–687.
46. Hasan, M.; Shang, Y.; Jin, W.; Akhter, G. Joint geophysical prospecting for groundwater exploration in weathered terrains of South Guangdong, China. *Environ. Monit. Assess.* **2021**, 193, 734. [[CrossRef](#)]

**Disclaimer/Publisher's Note:** The statements, opinions and data contained in all publications are solely those of the individual author(s) and contributor(s) and not of MDPI and/or the editor(s). MDPI and/or the editor(s) disclaim responsibility for any injury to people or property resulting from any ideas, methods, instructions or products referred to in the content.